Available online at www.sciencedirect.com
ScienceDirect
Journal of Sound and Vibration 297 (2006) 962–980
JOURNAL OF SOUND AND VIBRATION
www.elsevier.com/locate/jsvi

Theory and experiment on establishing the stability boundaries of a one-degree-of-freedom system under two high-frequency parametric excitation inputs

R.J. Yatawara, R.D. Neilson*, A.D.S. Barr

Department of Engineering, School of Engineering and Physical Sciences, University of Aberdeen, Aberdeen AB24 3UE, Scotland, UK

Received 3 August 2005; received in revised form 2 May 2006; accepted 3 May 2006
Available online 1 August 2006

Abstract

The stability of a single-degree-of-freedom linear system to two high-frequency parametric inputs is considered. Equations defining approximately the stability boundaries of the system are developed using Struble's method. The results of the analysis for a range of input frequency ratios and input amplitudes are compared with exact solutions for the regions of instability calculated from the monodromy matrix. Good agreement is found for low excitation levels. Experimental work involving the small amplitude oscillation of a pendulum under two frequency parametric motion is described, instability zones are found to exist and their stability boundaries shown to be reasonably close to those derived from the theory.

1. Introduction

The study of a linear single-degree-of-freedom system excited by a single parametric input has been studied extensively and the stability of such systems is well documented [1–4]. In practice however, in many instances parametric input signals are not steady periodic at a fixed frequency. In this paper, the effects of a fluctuating high frequency parametric excitation on the stability of a linear system is considered. The simplest case of an input, consisting of two sinusoidal signals with different frequencies and amplitudes, is investigated. The parametric input term can then be written as

$$f(t) = \gamma_1 \cos \Omega t + \gamma_2 \cos k\Omega t. \tag{1}$$

Of particular interest is the case with values of k around unity, which represents two inputs, close in frequency. In the case examined here the excitation frequencies, are considered to be much higher than the natural frequency p. Fig. 1 shows the typical beating waveform of such a parametric input.

The frequency of the beat or modulation is the difference $1/2(k-1)\Omega$ and the faster variations or carrier frequency within this envelope are near $1/2(k+1)\Omega$. The amplitudes γ_1 and γ_2 are the magnitudes of each input

*Corresponding author. Tel.: +44 1224 272797; fax: +44 1224 272 497.
E-mail address: r.d.neilson@eng.abdn.ac.uk (R.D. Neilson).

0022-460X/$ - see front matter © 2006 Elsevier Ltd. All rights reserved.
doi:10.1016/j.jsv.2006.05.008

Nomenclature

$f(t)$	two frequency parametric excitation input function	γ_1	forcing amplitude of input at frequency Ω
k	frequency ratio of the two inputs	γ_2	forcing amplitude of input at frequency $k\Omega$
p	natural frequency of system	ε	excitation level, small parameter for analysis
Q	non-dimensional natural frequency (p/Ω)	ε_1	excitation level of $\cos\tau$ input
t	time	ε_2	excitation level of $\cos k\tau$ input
x	coordinate, the displacement of the system	τ	non-dimensional time (Ωt)
y	relative excitation amplitude	Ω, $k\Omega$	frequencies of the two parametric inputs

and if these were equal the envelope would vary between zero and the maximum amplitude of the beat ($\gamma_1+\gamma_2$).

Previous work by McWhannel and Barr [5] and Othman and Watt [6] dealt mainly with a single value of k and was limited to inputs which were equal in size. Zounes and Rand [7] and Mitchell [8] also reported on a similar study, the latter based on the stable inverted pendulum, but with emphasis on the possible quasi-periodicity from an input of this form.

The results presented in this paper cover a range of values for k and differing relative amplitudes between the two frequency components. All values for k are taken to be rational in order to define a finite period. A parametric input of this type might be provided to a component mounted on the casing of a two-spool gas turbine aeroengine. The two shafts will provide two different frequencies to the base excitation of the component. If the component is flexibly mounted, for example, these frequencies might be high in relation to the natural frequency of the component on its mounting.

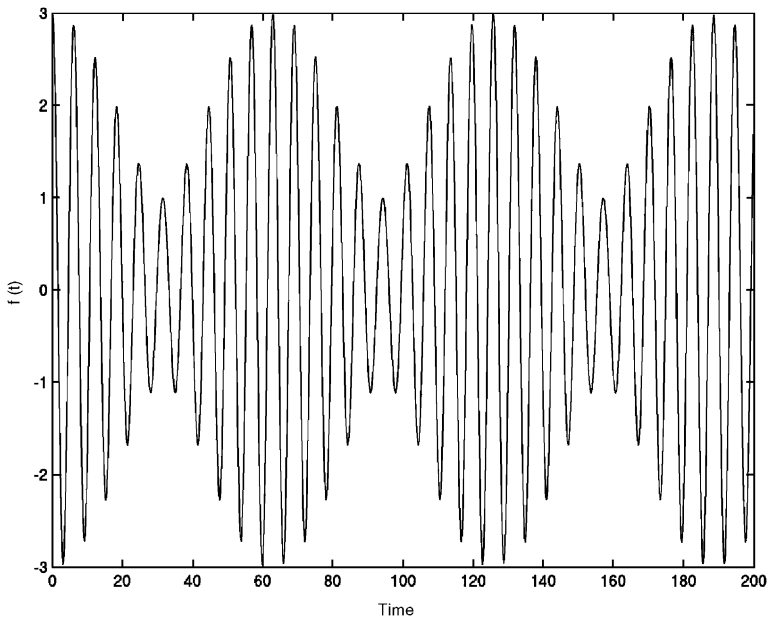

Fig. 1. Signal for two frequency inputs with $k = 1.1$ and $\gamma_1 = 2\gamma_2$.

2. Approximate stability boundary equations (originating at $2Q = (k-1)$)

The analysis is applied to a linear equation representing a single-degree-of-freedom system with the appropriate parametric excitation

$$\ddot{x} + (p^2 - \gamma_1 \cos \Omega t - \gamma_2 \cos k\Omega t)x = 0, \tag{2}$$

where p is the natural frequency, k is a constant taken to be >1 and the other parameters are as described for (1). Proceeding by non-dimensionalising (2) using the time-scaling

$$\tau = \Omega t \tag{3}$$

gives the acceleration in non-dimensionalised time τ as

$$\ddot{x} = \Omega^2 x'', \tag{4}$$

where the double prime denotes the second derivative with respect to τ. Expressing (2) in terms of τ gives

$$x'' + (Q^2 - \varepsilon_1 \cos \tau - \varepsilon_2 \cos k\tau)x = 0, \tag{5}$$

where the non-dimensional natural frequency and the excitation amplitudes are given by

$$Q = \frac{p}{\Omega} \tag{6}$$

and

$$\varepsilon_i = \frac{\gamma_i}{\Omega^2}. \tag{7}$$

Finally, in terms of an excitation amplitude ratio $y = \varepsilon_2/\varepsilon_1$ Eq. (5) can be written as

$$x'' + (Q^2 - \varepsilon \cos \tau - y\varepsilon \cos k\tau)x = 0, \tag{8}$$

where $\varepsilon = \varepsilon_1$ and $y\varepsilon = \varepsilon_2$.

A number of techniques, including the method of multiple scales, the method of slowly varying parameters and other perturbation procedures are available for the analysis of nonlinear and parametric systems [9]. In this case, the general asymptotic method developed by Struble [10] is used. The typical generating solution for this technique, which includes slowly varying amplitude $A(\tau)$ and phase $\phi(\tau)$, is expressed as

$$x(\tau) = A(\tau)\cos(Q\tau - \phi(\tau)) + \varepsilon u_1(\tau) + \varepsilon^2 u_2(\tau) + \ldots, \tag{9}$$

where u_1 and u_2 are the first and second terms in the asymptotic expansion, respectively.

Substituting (9) into (8) and neglecting terms of order ε^3 and higher gives

$$\begin{aligned}
&\left[\frac{d^2A}{d\tau^2} + 2QA\left(\frac{d\phi}{d\tau}\right) - A\left(\frac{d\phi}{d\tau}\right)^2\right]\cos(Q\tau - \phi) \\
&\quad + \left[2\left(\frac{dA}{d\tau}\right)\left(\frac{d\phi}{d\tau}\right) - 2Q\left(\frac{dA}{d\tau}\right) + A\left(\frac{d^2\phi}{d\tau^2}\right)\right]\sin(Q\tau - \phi) \\
&\quad + \left(\frac{d^2u_1}{d\tau^2} + Q^2u_1\right)\varepsilon + \left(\frac{d^2u_2}{d\tau^2} + Q^2u_2\right)\varepsilon^2. \\
&\quad = [A\cos(Q\tau - \phi)\cos\tau + Ay\cos(Q\tau - \phi)\cos k\tau]\varepsilon + [u_1\cos\tau + yu_1\cos k\tau]\varepsilon^2
\end{aligned} \tag{10}$$

The solution then proceeds by collecting terms in equal powers of ε and then sequentially solving these equations for u_1 and u_2. At each stage, where resonant terms are encountered these are removed from the equation being considered and added to the variational equations (order ε^0) which govern the slowly varying amplitude and phase. It can be seen that resonance conditions arise for $2Q = k \pm 1$. In this paper, the interest is centred on system excitation involving two high-frequency inputs. The resonance condition is $2Q = k - 1$ and all terms in the differential equations for u_1 and u_2 which have this frequency are moved to the variational

equations. This results in the following pair of variational equations:

$$\frac{\mathrm{d}A}{\mathrm{d}\tau} = \frac{\varepsilon^2}{4Q}\{[T + Py]\sin\theta\} \tag{11}$$

and

$$\frac{\mathrm{d}\theta}{\mathrm{d}\tau} = (k - 1 - 2Q) + \frac{\varepsilon^2}{2QA}\{[P + R + Sy + Ty] + [T + Py]\cos\theta\}, \tag{12}$$

where the original slowly varying phase ϕ has been redefined in terms of the new angle θ using

$$\theta = [(k - 1 - 2Q)\tau + 2\phi] \tag{13}$$

The variation of θ with respect to τ is then

$$\frac{\mathrm{d}\theta}{\mathrm{d}\tau} = (k - 1 - 2Q) + 2\frac{\mathrm{d}\phi}{\mathrm{d}\tau}. \tag{14}$$

The terms P, R, S and T in Eqs. (11) and (12) are given by

$$P = -\frac{A}{2(2Q + 1)}, \quad R = \frac{A}{2(2Q - 1)},$$
$$S = -\frac{Ay}{2(2Qk + k^2)}, \quad T = \frac{Ay}{2(2Qk - k^2)}.$$

If the slowly varying amplitude and phase are assumed to be constant on the boundaries of stability then $\mathrm{d}\theta(\tau)/\mathrm{d}\tau = 0$ and $\mathrm{d}A(\tau)/\mathrm{d}\tau = 0$ there, and from these the final approximate stability boundaries can be derived and are given by

$$2Q = (k - 1) - \frac{\varepsilon^2}{k(k - 1)} \times \left[\frac{(y^2 - 2y)k^2 - (2y^2 - 5y + 2)k - (2y - 1)}{(k - 2)(2k - 1)}\right] \tag{15}$$

$$2Q = (k - 1) - \frac{\varepsilon^2}{k(k - 1)} \times \left[\frac{(y^2 + 2y)k^2 - (2y^2 + 5y + 2)k + (2y + 1)}{(k - 2)(2k - 1)}\right]. \tag{16}$$

Eqs. (15) and (16) represent the two stability boundaries defining the limits of the unstable region for the resonance case $2Q = k-1$ with $k > 1$. These boundaries will be presented in the following section along with the exact instability regions as predicted using the monodromy matrix method [11]. A more complete presentation of the analysis undertaken to derive Eqs. (15) and (16) can be found in Ref. [12]. In the current work the monodromy matrix was obtained by integrating the full equation (Eq. (8)) over exactly one complete period of the forcing cycle. Two separate integrations with initial conditions (1,0) and (0,1) were used to produce the matrix for any particular set of parameters and the eigenvalues of this were then used to determine the stability of the system. This method is accurate to within the resolution of the integration procedure and the discretisation of the grid used to produce the shape of the unstable regions.

Expressions (15) and (16) have been derived, based on the assumption that $k > 1$. For $k < 1$, the original equation of motion, Eq. (8), can be transformed into an equation of similar form and equivalent expressions for the stability boundaries then result. The final form of the stability boundaries for $k < 1$ are included in Appendix A for completeness and are presented in terms of the current nomenclature.

3. Results

The following sections present the results generated using Eqs. (15) and (16) to provide the approximate stability boundaries of the system.

3.1. Effects of varying frequency ratio k

The initial calculations were undertaken to establish the effect of the frequency ratio k on the stability of the system. For these cases the relative amplitude of the two inputs was held constant with the same excitation amplitude for both i.e. $y = 1$. The level of excitation ε was varied and the non-dimensional natural frequency Q was varied relative to the two forcing frequencies of 1 and k. Graphs of the results are plotted with the excitation amplitude ε on the horizontal axis and the ratio $1/2Q$ on the vertical axis. In this presentation, the principal parametric region of the single input (Mathieu) equation emanates from $1/2Q = 1$ i.e. from the point where the excitation is twice the natural frequency. High values of $1/2Q$ indicate low values of natural frequency Q relative to the two forcing frequencies of 1 and k.

Fig. 2 shows the exact and approximate instability regions for the case where $k = 1.05$. In this and the following figures the unstable regions predicted by the monodromy matrix method are shaded. The boundaries of these shaded regions are smooth curves. The stepped appearance in the figures is due to the procedure used of scanning the roots of the monodromy matrix by varying the frequency ratio $1/2Q$ at discrete intervals of the excitation ε. The points on the stability boundaries predicted by Eqs. (15) and (16) are depicted by small crosses. The main resonance condition for infinitesimal ε occurs for $(k-1) = 2Q$ and should emanate from

$$\frac{1}{2Q} = \frac{1}{k-1} = \frac{1}{1.05-1} = 20. \tag{17}$$

As can be clearly seen from Fig. 2 this is the case. Both the exact regions calculated by the monodromy matrix method and the approximate region found using Struble's method start from $1/2Q = 20$ as predicted. Up to values of ε of around 0.02 the approximate and exact boundaries match well. Beyond this the solution produced by the asymptotic method diverges slightly, shifting to higher values of ε for the same excitation frequencies. The exact solution also shows the presence of a large number of other unstable regions. These occur from cases from other resonance conditions e.g. $2Q = 2(k-1)$ and are of higher order of ε. Although the analysis using the asymptotic solution was used to investigate only the case where $2Q = (k-1)$, the

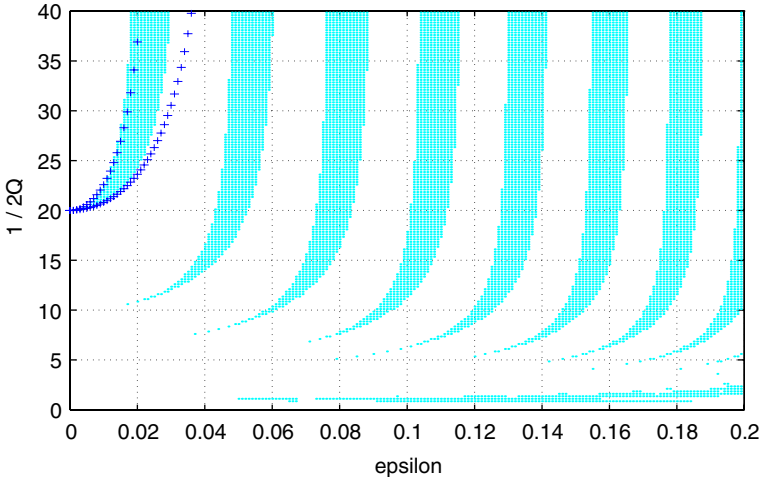

Fig. 2. Instability regions for two frequency inputs with $k = 1.05$, $y = 1.0$. Shaded areas denote unstable regions from monodromy matrix; + boundaries from Eqs. (15) and (16).

monodromy matrix method was applied to the full parameter space and therefore indicates all regions where there is unstable motion.

An interesting result of the analysis is that for most of the unstable regions, although they emanate from distinct points on the $1/2Q$ axis, once a certain level of excitation ε is achieved, provided the frequency ratio is above a certain level, the system will be unstable. The stability boundaries seem almost to tend towards lines of constant ε for large values of $(1/2Q)$. For example, for the region starting at $1/2Q = 20$, for an excitation $\varepsilon = 0.025$, instability appears to occur for all values of frequency above $1/2Q = 30$. Under such conditions the existence of parametric instability is very insensitive to the excitation frequencies. This tendency is also exhibited by the approximate boundaries but with reduced accuracy.

Figs. 3–5 show the exact and approximate stability regions for $k = 1.1$, 15 and 1.2. The form of the unstable regions is similar to those of Fig. 2 but it can also be seen that with increasing frequency ratio the unstable regions become wider and further apart and are shifted to higher excitation levels ε. For Fig. 3, the approximate upper stability boundary coincides with the exact region up to a value of $\varepsilon = 0.025$ while the lower boundary follows the exact region until about $\varepsilon = 0.03$. For Fig. 4, the approximate upper boundary is valid until about $\varepsilon = 0.04$ while the lower maintains good accuracy until about $\varepsilon = 0.06$. For the case where

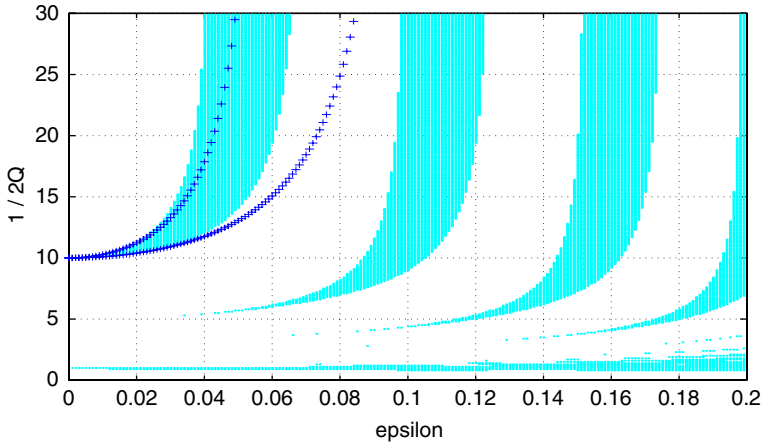

Fig. 3. Instability regions for two frequency inputs with $k = 1.1$, $y = 1.0$. Shaded areas denote unstable regions from monodromy matrix; + boundaries from Eqs. (15) and (16).

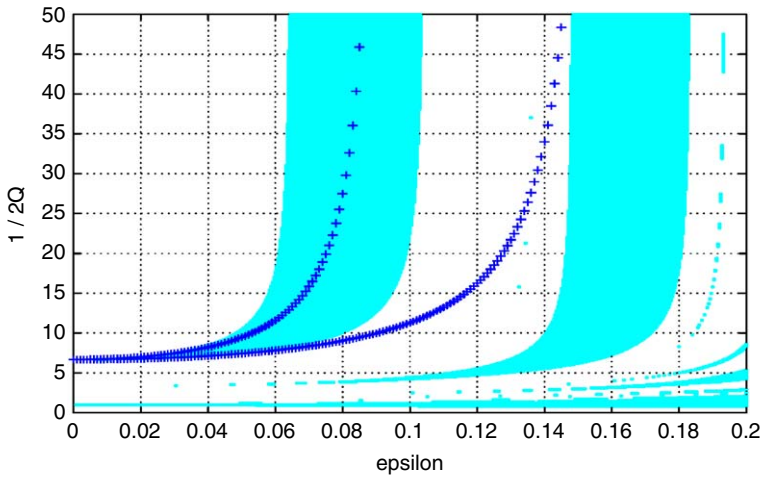

Fig. 4. Instability regions for two frequency inputs with $k = 1.15$, $y = 1.0$. Shaded areas denote unstable regions from monodromy matrix; + boundaries from Eqs. (15) and (16).

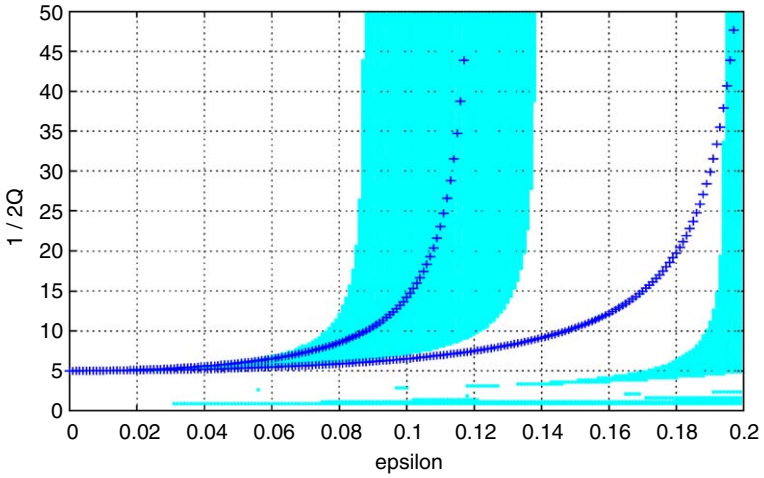

Fig. 5. Instability regions for two frequency inputs with $k = 1.2$, $y = 1.0$. Shaded areas denote unstable regions from monodromy matrix; + boundaries from Eqs. (15) and (16).

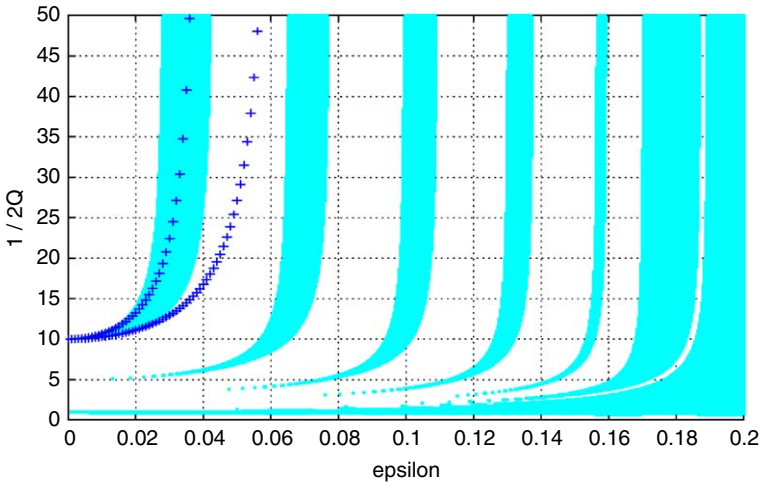

Fig. 6. Instability regions for two frequency inputs with $y = 2.0$, $k = 1.1$. Shaded areas denote unstable regions from monodromy matrix; + boundaries from Eqs. (15) and (16).

$k = 1.2$ (Fig. 5) the upper and lower approximate solutions are valid up to values of $\varepsilon = 0.06$ and 0.08, respectively.

The case of $k = 1$ has not been considered as it corresponds to the single input case which is already well documented in the literature and is not relevant to the present study.

3.2. *Effects of varying the relative input amplitude y*

Figs. 6–9 present the approximate and exact instability results generated for y values of $y = 2$, $1/2$, 4 and $1/4$, respectively, with k fixed at 1.1 in all cases. The objective here is to investigate the difference between stability when the input of the higher frequency $k\Omega$ is bigger in amplitude ($y > 1$) than the primary input Ω, and also when it is smaller ($y < 1$).

Comparing Fig. 6 with Fig. 7 and Fig. 8 with Fig. 9 it is evident that the area of each instability zone common to both cases, in the region shown, is smaller when the amplitude y of the higher frequency $k\Omega$ is larger, but although the regions are narrower for larger y they are greater in number. Additionally for $y > 1$ the first stability boundary at high excitation frequency e.g. $1/2Q = 30$ is encountered for lower ε at greater y,

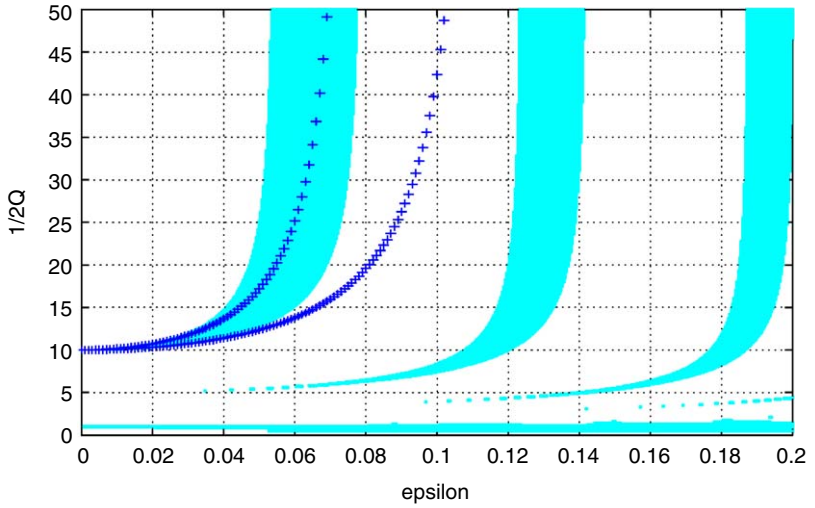

Fig. 7. Instability regions for two frequency inputs with $y = 1/2$, $k = 1.1$. Shaded areas denote unstable regions from monodromy matrix; + boundaries from Eqs. (15) and (16).

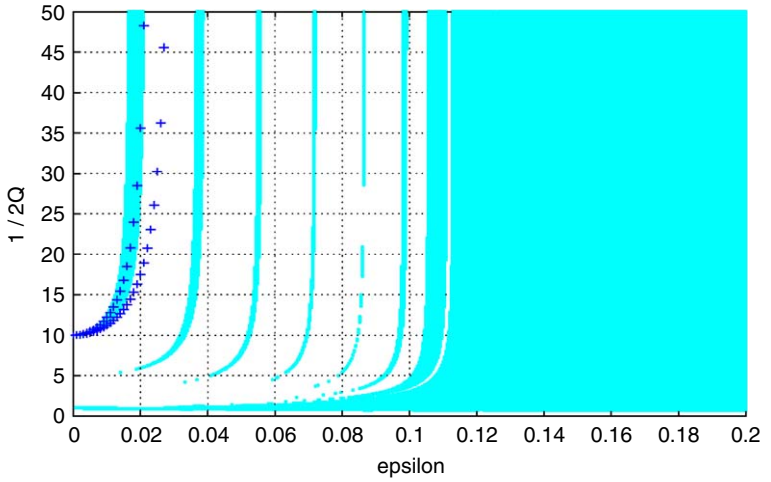

Fig. 8. Instability regions for two frequency inputs with $y = 4.0$, $k = 1.1$. Shaded areas denote unstable regions from monodromy matrix; + boundaries from Eqs. (15) and (16).

making it perhaps of more practical significance. The same relative amplitude levels y were studied for other values of k, showing similar trends in the stability diagrams.

The changes in the instability regions, as y is varied, can also be visualised for a particular frequency ratio $1/2Q$ as depicted in Fig. 10. The instability regions depicted in this diagram correspond to a sum of cross sections from diagrams, such as the preceding, computed at $1/2Q = 13.5$. Presentation of this diagram is on an ε versus $y\varepsilon$ plane, a third ordinate normal to the paper can be visualised representing the frequency ratio $1/2Q$. The four lines drawn in Fig. 10 then correspond to the planes of the earlier Figs. 3 and 6–9 for the particular values of y. For each y, the width of any instability area intersected corresponds to the width of the corresponding instability zone, at the specified frequency ratio of $1/2Q = 13.5$, in the relevant diagram. Combined, the stability diagrams presented in the various planes of constant y give a general indication of the shape and distribution of these high multifrequency instability regions in the three-dimensional parameter space, ε, $y\varepsilon$ and $1/2Q$.

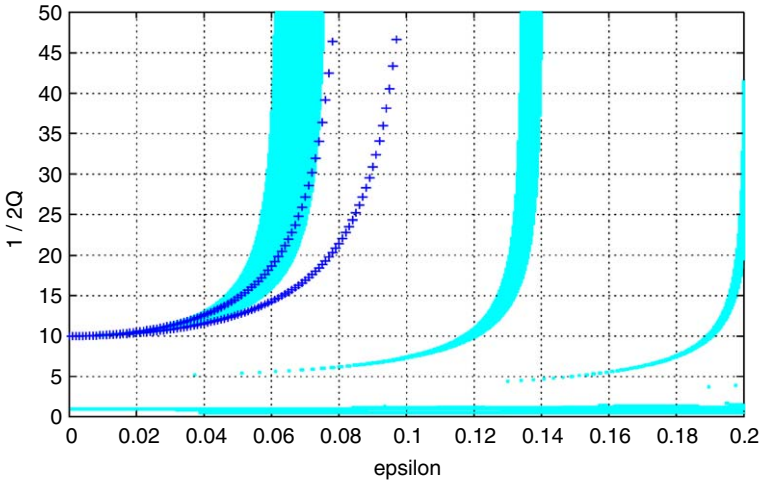

Fig. 9. Instability regions for two frequency inputs with $y = 1/4$, $k = 1.1$. Shaded areas denote unstable regions from monodromy matrix; + boundaries from Eqs. (15) and (16).

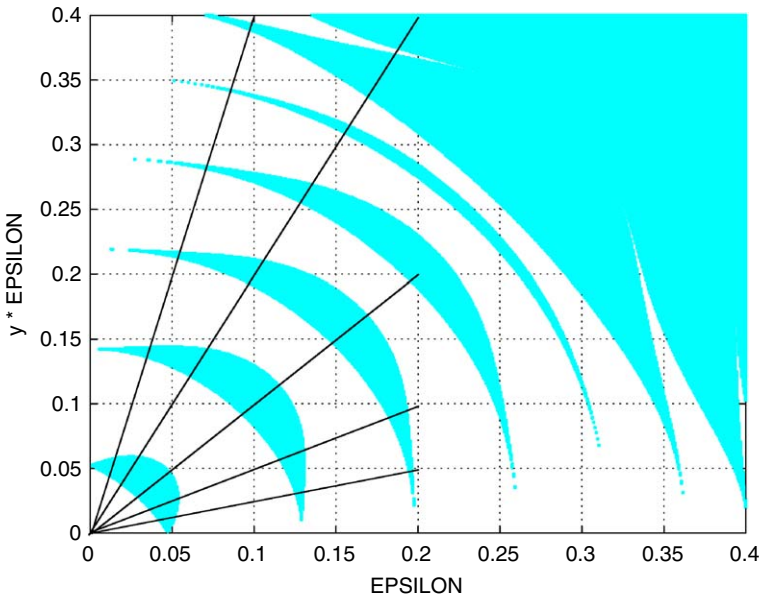

Fig. 10. Instability regions from monodromy matrix for two frequency inputs, magnitudes ε and $y\varepsilon$ with $k = 1.1$ at $1/2Q = 13.5$ (i.e. $\Omega/2P = 13.5$). Shaded areas denote unstable regions.

3.3. *Effect of including viscous damping*

The effects of viscous damping previously reported for parametric systems in general, also apply to this particular case. From Figs. 11 and 12, in which viscous damping with damping ratio v was introduced into Eq. (8), it can be seen that the tip of the unstable region moves away from the axis $\varepsilon = 0$ and the stability boundaries are contained within those for zero damping, thus the unstable regions shrink as the damping ratio is increased.

3.4. *Final remarks*

The diagrams presented help to provide a general understanding of the stability behaviour to be expected in a linear single degree of freedom system which is parametrically excited by two frequencies which are relatively

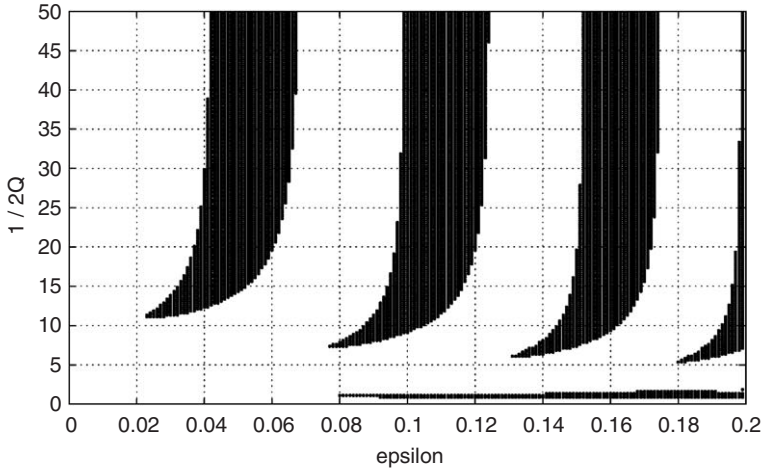

Fig. 11. Instability regions from monodromy matrix for two frequency inputs with $k = 1.1$, $y = 1.0$ and $v = 0.05$. Shaded areas denote unstable regions.

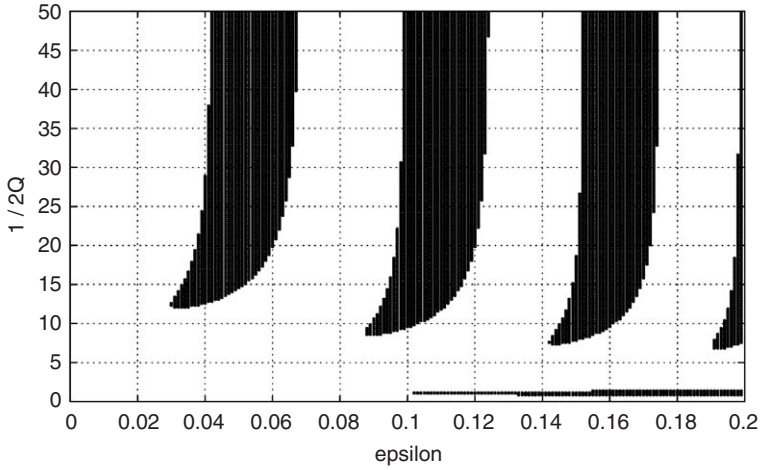

Fig. 12. Instability regions from monodromy matrix for two frequency inputs with $k = 1.1$, $y = 1.0$ and $v = 0.1$. Shaded areas denote unstable regions.

close but are high compared to the natural frequency p. Stability diagrams for varying relative frequency (k) between the two components confirm the increase in the potential for encountering an unstable response when the two frequencies are very close ($k \to 1$). This was also observed by Bogandoff and Citron [1] and Dugundji and Chatpar [5].

For very small values of ε the approximate boundaries compare well with the accurate results obtained using the monodromy matrix method. Both results originate from the predicted resonant condition and in most cases remain close until ε is around 0.04. Thereafter, as ε gets larger the approximate unstable region drifts to higher excitation ε. The accurate boundaries appear to tend to vertical asymptotes. To obtain approximations for the higher order regions the Struble analysis has to be extended to a higher order of ε. There is no conclusive evidence to show that extension to such higher-order approximation will improve the accuracy of the lower order regions, although this does seem likely. The Struble results also seem to approximate better the exact unstable zones further away from the principal parametric regions of instability.

The regions of instability associated with the principal parametric resonance of each input taken separately originate at low frequency ratios $(\Omega/2p) \approx 1$ or k. In the graphs presented these regions remain narrow until ε is relatively large and therefore can be avoided by a slight shift in excitation frequency Ω whereas with two inputs

acting jointly as considered here each region has a range of ε within which instability will result almost irrespective of the frequency ratio of excitation to natural frequency.

4. Experimental study

There is an extensive amount of experimental work reported on different aspects of parametric systems, however the few that deal with high-frequency parametric excitation have been very limited in providing conclusive experimental data. In the majority of these cases the difficulty has been in limiting the response or resonance to that of a single mode or to the required mode. McWhannel and Barr [5] report attempting to excite the main resonance condition governed by the difference between the two close frequencies. Utilising a slender beam with low damping they was able to find instability although maintaining the single mode and the precise excitation conditions required, proved difficult. Miyasar and Barr [13], as with the theoretical study, limited experimental work to frequencies near the Mathieu regions of instability. Related experimental work was also reported in Refs. [1,14].

Considering the difficulties reported in the literature for previous experimental work, the key factor when designing the test rig for this study was the restriction of the response to that of the single mode under consideration. For this reason a rigid pendulum type of rig was decided upon with the rigid body mode well separated from the elastic modes.

4.1. Equation of motion of a pendulum subject to base excitation

Prior to embarking on the design of the rig it was necessary to ensure that the equation of motion representing the experimental system corresponded to that being studied. The equation of motion for oscillations of a compound pendulum subject to support acceleration excitation $\ddot{u}$ in the upward vertical direction is

$$\ddot{\theta} + \left(\frac{M_{\text{eff}} gh}{I_o} + \frac{M_{\text{eff}} h\ddot{u}}{I_o}\right) \sin\theta = 0, \tag{18}$$

where M_{eff} is the effective mass of the equivalent simple pendulum having the same natural frequency; for small θ

$$\ddot{\theta} + \left(\frac{M_{\text{eff}} gh}{I_o} + \frac{M_{\text{eff}} h\ddot{u}}{I_o}\right)\theta = 0 \tag{19}$$

or

$$\ddot{\theta} + p^2\left(1 + \frac{\ddot{u}}{g}\right)\theta = 0, \tag{20}$$

where

$$p = \sqrt{\frac{M_{\text{eff}} gh}{I_o}}. \tag{21}$$

Substituting as in Eq. (1)

$$\ddot{u}(t) = -\gamma_1 \cos \Omega t - \gamma_2 \cos k\Omega t \tag{22}$$

produces an equation of the form presented in Eq. (2).

4.2. Design and features of test rig

The choice of a rigid pendulum rig allows the required low first natural frequency to be designed in. It also improves the ability to attain high forcing frequency ratios (Ω/p) and ($k\Omega/p$). Although a long pendulum rod would have been the obvious choice for attaining the low natural frequency sought, this would have increased

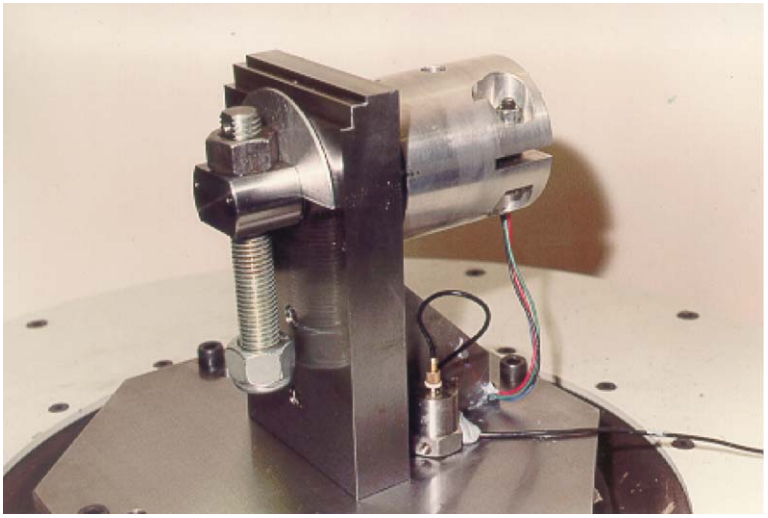

Fig. 13. View of the experimental rig.

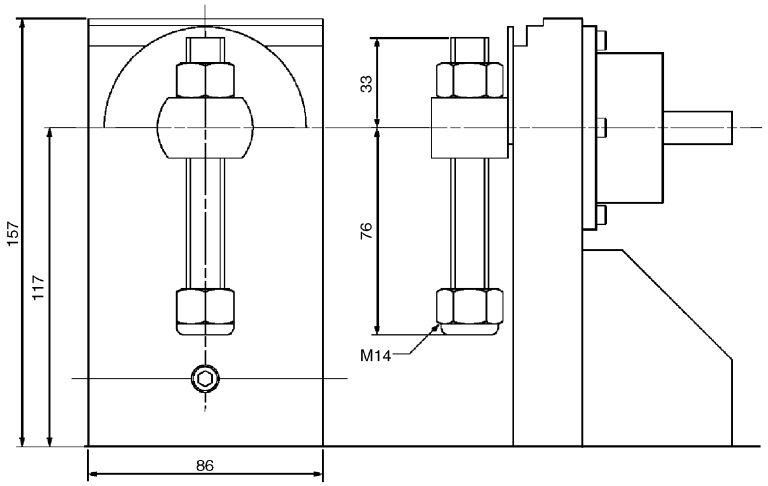

Fig. 14. Dimensions of pendulum rod.

the potential for exciting the flexible modes of the long slender rod. Additionally, the overall size of the rig had to be kept to a minimum in order to reduce the payload on the shaker of the system used for excitation.

The final design of the rig is presented in Fig. 13. It comprises a vertical plate with a flanged cylindrical bearing housing bolted on to the back of it. These two components house the main spindle and the angular contact bearings, which support it. The rod, which acts as the main member of the pendulum, is threaded through the hub at the end of the spindle and is held in place by a lock nut.

A rotary transducer is contained in the large cylindrical housing seen at the rear of the rig in Fig. 13. This fits on to the free end of the bearing housing and is held in place by two grub screws. The transducer is inserted into the housing through a bore at the open end and is secured in place by the bolts, which can be seen in Fig. 13. When fully inserted a key seat on the shaft of the rotary transducer sits within a small bore at the end of the main spindle and the two are locked together by a grub screw. The output range of the transducer is only from 0° to $\pm 90^\circ$, and therefore to be able to identify the response when the pendulum is outside the bottom half of its response circle, a semi-circular disc was added to the design. A signal from an optical switch (not shown in the preceding figure), which is activated and deactivated by this disc, is used together with the transducer signal to track the pendulum. The dimensions of the rig are shown in Fig. 14.

The base excitation was measured and monitored by an accelerometer and its spectral composition was displayed on an HP 3582 spectrum analyser. An oscilloscope was also used in conjunction with the analyser to display the time history, confirming the form of the parametric excitation. The data from the angular transducer and the optical switch were fed into a data acquisition unit, which was controlled/configured, by WAVECAP software. Settings such as sampling rate, scale factors and offsets were all specified in this software.

As seen from the derived expression (21) the natural frequency p is required for setting the required frequency ratio and for ascertaining the amplitude of the parametric term from the measured acceleration. The pendulum was allowed to oscillate freely and the response from the angular transducer, was fed into the HP3582. The response frequency measured on the analyser was $p = 1.72$ Hz. Data points from the same response were used to estimate the inherent damping in the rig using the logarithmic decrement. From this the equivalent viscous damping ratio was estimated to be $v = 0.025$. The main contributor to damping is the friction in the transducer and in the ball bearings.

Two WAVETEK model 75 Arbitrary Waveform Generators were used in series to generate the input waveform to the shaker. When the output from one generator is connected to the 'Sum In' of the other the result is a waveform which is a summation of the two, in this case a beating waveform as shown. The absolute amplitude of each frequency component is governed by the first generator and the ratio between the two amplitudes is set by the second, a maximum setting giving a 1:1 ratio. With the digital type controls on these signal generators, precise adjustments could be made to the output waveform.

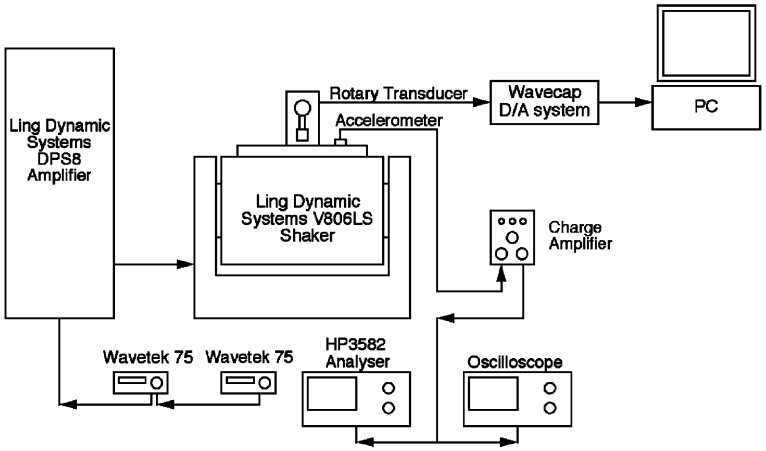

Fig. 15. General schematic of the experimental system.

Table 1
Parameter combinations studied experimentally—two close frequencies

Figure	k	y	Ω range—[1/2Q]
16	1.05	1	36.12–51.6 Hz—[10.5–15.0]
17	1.1	1	68.8–86 Hz—[20–25]
18	1.2	1	18.92–27.52 Hz—[5–8]
19	1.1	2	37.84–51.6 Hz—[11–15]
20	1.1	1/2	37.84–49.88 Hz—[11–14.5]
21	1.1	1	Fixed at 46.44 Hz—[13.5]
		2	
		0.5	

$p = 1.72$ Hz.

Monitoring and measuring the excitation of the base of the test rig was carried out using an accelerometer, which was attached to the shaker head and fed to the HP 3582 analyser. This allowed accurate confirmation of both frequency and amplitude of the base acceleration. A schematic of the instrumentation and control system is presented in Fig. 15. The parameters used for the experimental tests are shown in Table 1 for each of the Figures presenting the results, which follow.

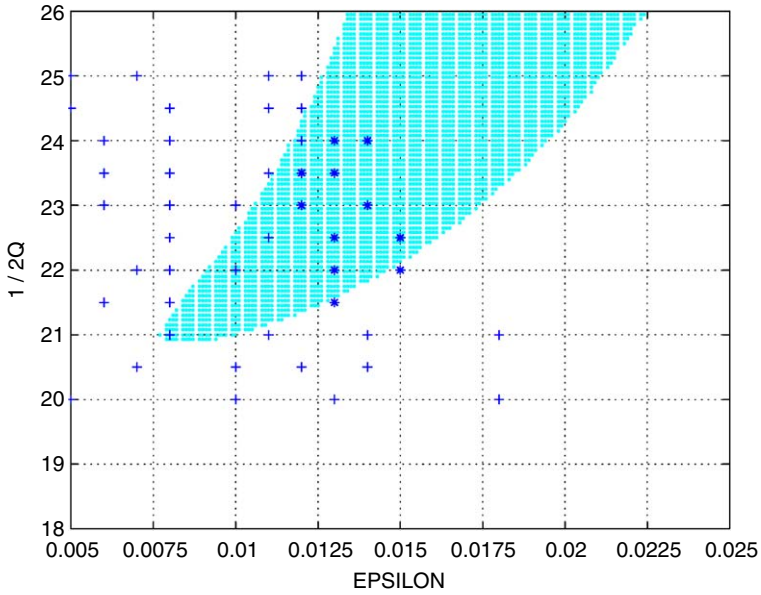

Fig. 16. Experimental results for two frequency inputs with $k = 1.05$ and $y = 1.0$ (+*stable*; **unstable*). Shaded areas denote unstable regions from monodromy matrix, including damping.

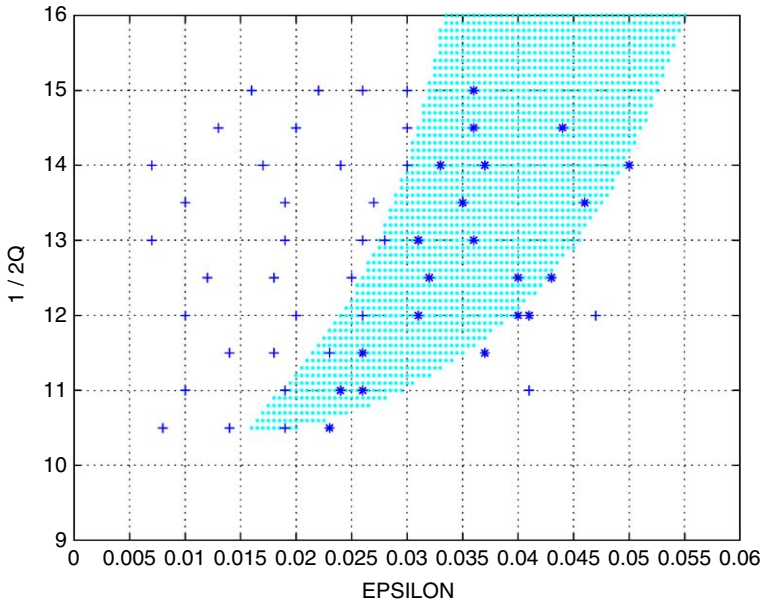

Fig. 17. Experimental results for two frequency inputs with $k = 1.1$ and $y = 1.0$. (+*stable*; **unstable*). Shaded areas denote unstable regions from monodromy matrix, including damping.

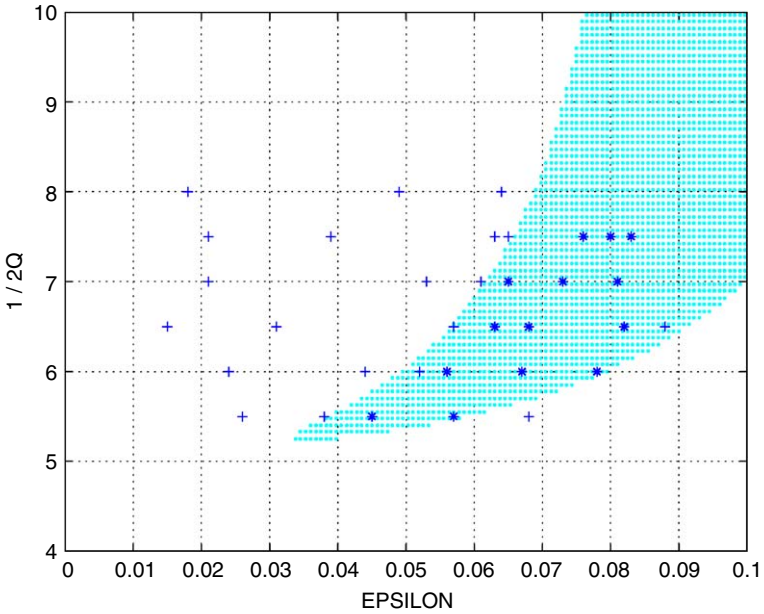

Fig. 18. Experimental results for two frequency inputs with $k = 1.2$ and $y = 1.0$ (+*stable*; **unstable*). Shaded areas denote unstable regions from monodromy matrix, including damping.

4.3. Experimental results for varying k

Figs. 16–18 show the experimental results for $y = 1$ and $k = 1.05$, 1.1 and 1.2, respectively, superimposed on the unstable regions as calculated using the monodromy matrix. In this case, the exact regions were calculated using the value of damping of $v = 0.025$ found during testing.

Comparing the results of the experiment with those of the exact solution reveals good agreement for all three cases. The majority of the experimental results lie clearly within the bounds of the exact unstable regions. The few points, which do not agree with the exact boundaries, all lie close to the boundaries themselves and all are shifted to the right of the exact boundaries i.e. to higher values of ε. This slight shift is thought to be due to the softening nonlinearity present in the experimental system, which is not included in the linear theoretical model. Because it is possible to determine the onset of instability in an experimental system only with a finite oscillation, such nonlinearities may influence the apparent boundaries. In this case however the difference in the results is small and the experimental results can be said to validate the model.

With growing amplitude θ the linearity in Eq. (21) no longer holds and it is useful, particularly in the analysis of experimental results, to be aware of modifications to the instability regions when the nonlinear terms are retained in the equation, in this case though the term $\sin\theta$ of Eq. (19).

The amplitude of the response tends to be limited, although often in reality to an unacceptably large value, because of the characteristic 'bend-over' of the nonlinear response curves. As result the boundaries of stability are amplitude dependant, which can be seen clearly by generating a three-dimensional stability map which also incorporates the amplitude of the response. Reference can be made to the frequency response curves described in Refs. [2,3] in the analysis of the periodic responses of a simple pendulum under pure sinusoidal mono-frequency base excitation. The general form of such a response curve is shown in Fig. 19 as an example.

The hatched area is the principal parametric instability region where the null solution, $\theta = \dot{\theta} = 0$, is unstable. Without the nonlinearity, the solution within this zone will grow to infinity from a small initiation, but as shown in Fig. 19 the final amplitude of the solution is limited by the upper bounding curves, which are denoted by a solid line. Solution points such as B on the lower bounding curves (dashed lines) are not stable and the response will either rise to C or collapse to A depending on the initial conditions. This structure of the nonlinear response curves introduces some complexities when attempting experimentally to establish the instability zones for small amplitudes.

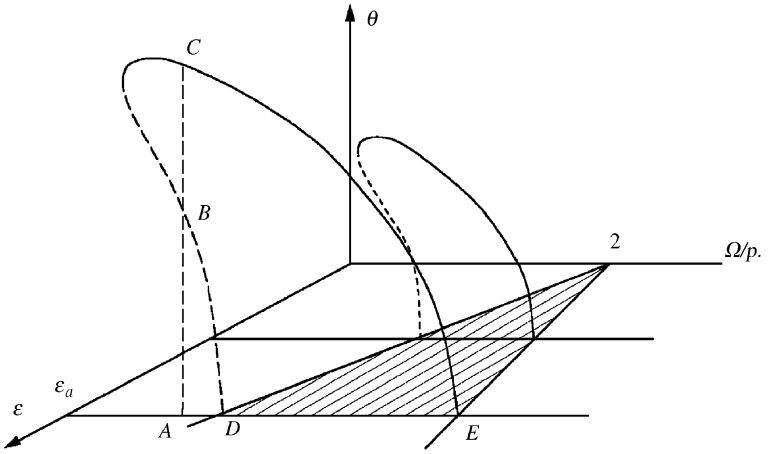

Fig. 19. Nonlinear response curves for a simple pendulum with natural frequency p under single frequency excitation Ω.

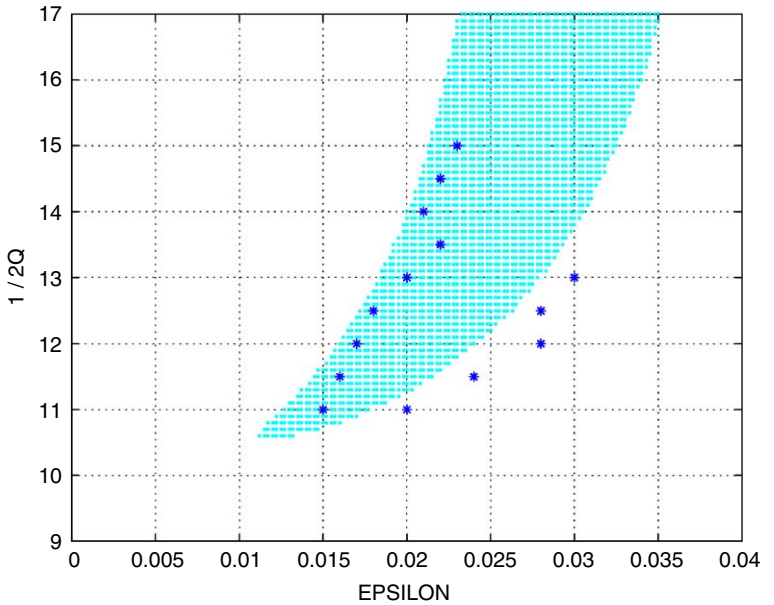

Fig. 20. Experimental unstable points defining the boundaries for two frequency inputs with $k = 1.1$ and $y = 2.0$. Shaded areas denote unstable regions from monodromy matrix, including damping.

Under an excitation amplitude of ε_a if the frequency is increased to A, a small disturbance will decay to rest. If however the initial condition is large enough the resulting solution amplitude will generally rise to C. Increasing the frequency just beyond D will generate an amplitude on the solid line EC in response to very small initial conditions. Detecting the onset of instability when reducing the frequency down to E is not easy since a large amplitude solution will not be generated until the frequency is reduced well into the unstable zone.

4.4. Results for varying y

This section describes the experimental results essentially defining the boundaries of the first unstable zone for two different values of excitation amplitude ratio y. Figs. 20 and 21 show the experimental results for $k = 1.1$ and $y = 2.0$ and $1/2$, respectively, superimposed on the regions calculated using the monodromy

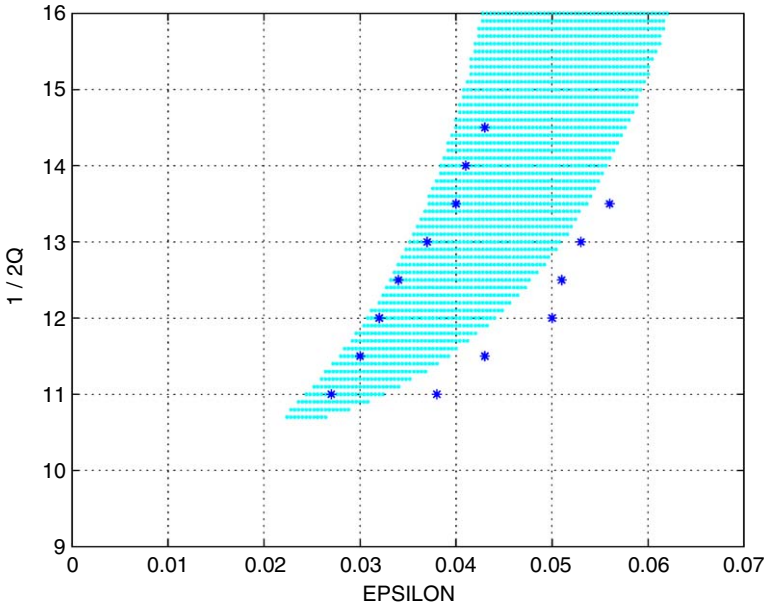

Fig. 21. Experimental unstable points defining the boundaries for two frequency inputs with $k = 1.1$ and $y = 1/2$. Shaded areas denote unstable regions from monodromy matrix, including damping.

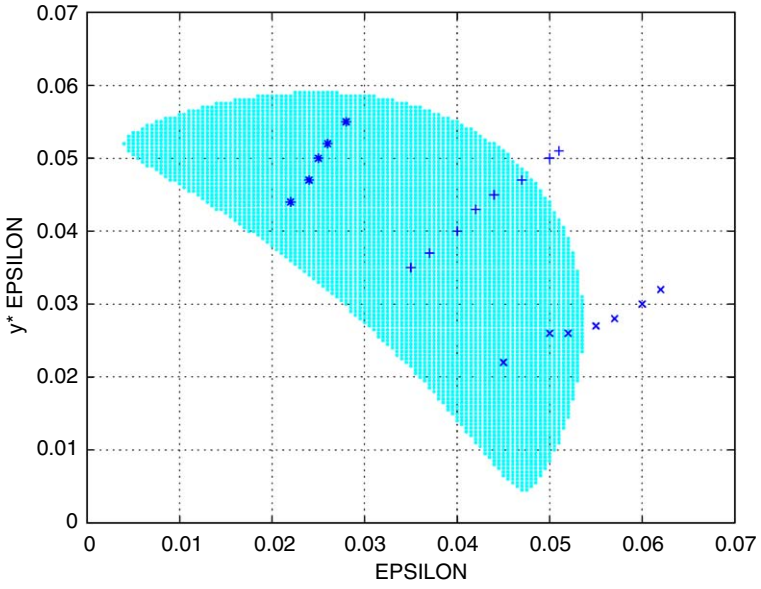

Fig. 22. Experimental unstable points for two frequency inputs with $k = 1.1$, $y = 1.0$ (+), 2.0 (*), & 0.5 ($\times$) and $1/2Q = 13.5$. Shaded areas denote unstable regions from monodromy matrix, including damping.

matrix. Again reasonably good agreement is apparent, with the main differences between the results for the exact and experimental boundaries being a slight shift to the right for the latter. This is again attributed to the nonlinearity in the experimental system.

In Fig. 22, a further set of experimentally obtained unstable points at fixed excitation frequency $1/2Q = 13.5$ and $k = 1.1$ for varying amplitudes of excitation ε and $y\varepsilon$ are shown against the calculated regions similar to those already described in Fig. 10. This was chosen as it was one of the highest frequency levels that could

be achieved with the shaker system and the pendulum being tested for all values of y. The value of $1/2Q = 13.5$corresponds to a true excitation frequency Ω of 46.4 Hz.

The results depicted in Fig. 22 show again that for these cases with varying amplitude ratio y, the experimental and exact unstable regions agree reasonably well. The case for $y = 1/2$ shows the worst correlation where again the unstable region is moved to higher values of ε.

5. Conclusions

The stability boundaries for a single degree of freedom system subject to parametric excitation by an input with two frequencies which are close but are high relative to the natural frequency have been obtained approximately using Struble's method, exactly using monodromy matrix and experimentally using a laboratory rig.

The results show that the unstable regions examined emanate from $2Q = (k-1)$ where Q is the ratio of the natural frequency and the lower of the excitation frequencies and k is the ratio of the two input frequencies. These regions then expand initially with increasing excitation level ε. However, beyond a certain level of excitation, ε, the system is relatively insensitive to the value of the excitation frequencies and unstable regions exist over a wide range of excitation frequencies.

The theoretical approximations given by Struble's method agree quite well with the precise computation from the use of the monodromy matrix but only for small values of the excitation parameter ε. Experimental work demonstrates the physical existence of these instabilities and shows satisfactory correspondence with the predictions of theory.

Appendix A. Approximate stability boundaries (Eqs. (15) and (16)) for $k<1$

The original equation is of the form

$$x'' + \left[Q^2 - \varepsilon(\cos\tau + y\cos k\tau)\right]x = 0. \tag{A.1}$$

For cases where $k<1$ then the approximate stability boundaries obtained using Struble's method can be shown to be

$$2Q = (1-k) - \frac{\varepsilon^2}{k(1-k)} \times \left[\frac{(y^2-2y)k^2 - (2y^2-5y+2)k - (2y-1)}{(2-k)(1-2k)}\right] \tag{A.2}$$

$$2Q = (1-k) - \frac{\varepsilon^2}{k(1-k)} \times \left[\frac{(y^2+2y)k^2 - (2y^2+5y+2)k + (2y+1)}{(2-k)(1-2k)}\right]. \tag{A.3}$$

References

[1] J.L. Bogandoff, S.J. Citron, Experiments with an inverted pendulum subjected to random parametric excitation, *Journal of the Acoustical Society of America* 38 (1965) 447–452.

[2] D. Capecchi, S.R. Bishop, Periodic oscillations and attracting basins for a parametrically excited pendulum, *International Journal of Dynamics and Stability of Systems* 9 (2) (1994) 123–143.

[3] F. Curzo, et al., Parametric instability of a pendulum, *American Journal of Physics* 63 (2) (1995) 132.

[4] J. Dugundji, C.K. Chatpar, Dynamic stability of a pendulum under parametric excitation—Air Force Office of Scientific Research, Scientific Report,1968.

[5] D.C. McWhannell, A.D.S. Barr, Parametric instability in structures under support motion, *Journal of Sound and Vibration* 14 (4) (1971) 491–509.

[6] A.M. Othman, D. Watt, A.D.S. Barr, Stability boundaries of an oscillator under high frequency multi-component parametric excitation, *Journal of Sound and Vibration* 112 (2) (1987) 249–259.
[7] R.S. Zounes, R.H. Rand, Transition curves in the quasiperiodic Mathieu equation, *Nonlinear Dynamics and Controls, ASME* 91 (1996) 1–6.
[8] R. Mitchell, Stability of the inverted pendulum subjected to almost periodic and stochastic base motion—an application of the method of averaging, *International Journal of Non-linear Mechanics* 7 (1972) 101–123.
[9] A.H. Nayfeh, *Perturbation Methods*, Wiley-Interscience, New York, 1973.
[10] R.A. Struble, *Nonlinear Differential Equations*, McGraw-Hill, New York, 1962.
[11] L.A. Pars, *A Treatise on Analytical Dynamics*, Heinemann, London, 1964.
[12] R.J. Yatawara, Single Degree of Freedom Instability Under High Multi-frequency and Nonstationary Parametric Excitations, PhD Thesis, Aberdeen University, Aberdeen, UK, 2000.
[13] A.M. Miyasar, A.D.S. Barr, The linear oscillator under parametric excitation with fluctuating frequency, *Journal of Sound and Vibration* 124 (1) (1988) 79–89.
[14] G.W. Hemp, P.R. Sethna, On dynamical systems with high frequency parametric excitation, *International Journal of Non-linear Mechanics* 3 (1968) 351–365.